Crystal Structure of β-Carbonic Anhydrase CafA from the Fungal Pathogen *Aspergillus fumigatus*

Subin Kim, Jungyoon Yeon, Jongmin Sung, and Mi Sun Jin*

School of Life Sciences, Gwangju Institute of Science and Technology (GIST), Gwangju 61005, Korea
*Correspondence: misunjin@gist.ac.kr
https://doi.org/10.14348/molcells.2020.0168
www.molcells.org

The β-class of carbonic anhydrases (β-CAs) are zinc metalloenzymes widely distributed in the fungal kingdom that play essential roles in growth, survival, differentiation, and virulence by catalyzing the reversible interconversion of carbon dioxide (CO_2) and bicarbonate (HCO_3^-). Herein, we report the biochemical and crystallographic characterization of the β-CA CafA from the fungal pathogen *Aspergillus fumigatus*, the main causative agent of invasive aspergillosis. CafA exhibited apparent *in vitro* CO_2 hydration activity in neutral to weak alkaline conditions, but little activity at acidic pH. The high-resolution crystal structure of CafA revealed a tetramer comprising a dimer of dimers, in which the catalytic zinc ion is tetrahedrally coordinated by three conserved residues (C119, H175, C178) and an acetate anion presumably acquired from the crystallization solution, indicating a freely accessible "open" conformation. Furthermore, knowledge of the structure of CafA in complex with the potent inhibitor acetazolamide, together with its functional intolerance of nitrate (NO_3^-) ions, could be exploited to develop new antifungal agents for the treatment of invasive aspergillosis.

Keywords: β-class carbonic anhydrase, *Aspergillus fumigatus*, CafA, X-ray crystallography, zinc metalloenzyme

INTRODUCTION

Carbonic anhydrases (CAs) are widely distributed zinc metalloenzymes that catalyze the interconversion of carbon dioxide to bicarbonate and a proton (Supuran, 2016). They are currently divided into seven families (α, β, γ, δ, ζ, η, θ), which are evolutionarily unrelated in amino acid sequence and structure (Del Prete et al., 2014a; 2014b; Iverson et al., 2000; Kikutani et al., 2016; Meldrum and Roughton, 1933; Mitsuhashi et al., 2000; Xu et al., 2008). Of the different classes, α- and β-CAs have been well-characterized biophysically and structurally. α-CAs are found in mammals, fungi, prokaryotes, and plants. All known bacterial α-CAs are dimers (Kim et al., 2019b; Kimber and Pai, 2000), while most mammalian CAs are monomers, with some also possessing dimeric α-CA forms (Alterio et al., 2009; Pilka et al., 2012; Whittington et al., 2001). α-CAs have a catalytic zinc ion coordinated by three conserved histidine residues and a water molecule (or hydroxide ion) in their active sites (Nair et al., 1995). Extensive structural and biochemical analysis has led to the two-step CO_2 hydration model for the α-CA family (Silverman and Lindskog, 1988). In this model, the first step is initiated by zinc ion, which promotes the ionization of bound H_2O and results in nucleophilic attack on CO_2 to generate hydrated carbon dioxide (bicarbonate, HCO_3^-). The second step is the transfer of a proton from bulk solvent to the zinc-bound hydroxide ion, regenerating the zinc-bound water and resetting the enzyme. In this process, H64 (in human α-CA II) acts as a proton shuttle via a side chain movement from "in" (pointing toward the active site) to "out" (pointing toward the solvent) (Fisher et al., 2007; Maupin and Voth, 2007; West et al., 2012). In the past decade, highly thermo- and alkali-stable

α-CA enzymes from mycobacteria and algae have attracted great attention for mitigating global warming because biomineralization of CO_2 using these enzymes is one of the most economical ways of permanently storing carbon (Capasso et al., 2012b; Jo et al., 2014; Luca et al., 2013; Russo et al., 2013).

β-CAs were first discovered in plant leaf chloroplasts, but have since been found in bacteria, fungi, and algae (Neish, 1939; Smith et al., 1999). Based on the amino acid sequence and structure, they are divided into two main subgroups: plant-type tetramers such as that in *Pisum sativum*, and the cab-type dimer such as that in *Methanobacterium thermoautotrophicum* (Kimber and Pai, 2000; Smith and Ferry, 1999; Strop et al., 2001). In the fungal kingdom, members of the β-class of carbonic anhydrases play a key role in growth, development, virulence, and survival, although some fungi also possess α-CAs (Elleuche and Pöggeler, 2010). In hemiascomycetous yeasts, the Nce103 gene encoding a single copy of a plant-type β-CA is required for growth under ambient conditions but is dispensable for pH homeostasis at high CO_2 levels (Götz et al., 1999; Innocenti et al., 2009; Klengel et al., 2005). By contrast, basidiomycetes and filamentous ascomycetes possess multiple CA isoforms with different cellular locations and catalytic efficiency. For example, two closely related β-CAs, Can1 and Can2, have been identified in *Cryptococcus neoformans* and *Cryptococcus gatti*, but only Can2 has been shown to be crucial for growth under ambient CO_2 conditions (Bahn et al., 2005; Ren et al., 2014). In *Sordaria macrospora*, four β-CAs have been identified (CAS1-4), and only deletion of CAS2 had a severe effect on vegetative growth and ascospore germination, indicating that CAS2 is the major β-CA (Elleuche and Pöggeler, 2009).

The functions of four β-CAs (CafA-D) also have been determined in *Aspergillus fumigatus*, the main causative agent of invasive aspergillosis (Han et al., 2010). CafA and CafB are closely related proteins that belong to plant-type tetrameric β-CAs, whereas CafC and CafD are classified as cab-type dimeric enzymes. *In silico* sequence analysis predicted that CafA and CafD are translocated into mitochondria, whereas CafB and CafC are cytoplasmic. Analysis of deletion mutants showed that CafA and CafB genes are constitutively and strongly expressed, whereas CafC and CafD are weakly expressed but induced by high CO_2 concentrations. Furthermore, only the double deletion mutant lacking CafA and CafB was unable to grow under ambient CO_2 concentrations. These results suggest that CafA and CafB are the major β-CAs in *A. fumigatus*, whereas CafC and CafD are minor β-CAs in this organism.

Recently, we solved the crystal structures of CafC and CafD by X-ray crystallography (Kim et al., 2019a). Using these structures, combined with our biochemical data, we revealed the molecular basis underlying their low activities. In CafC, access of CO_2 to the active site is limited by a narrow opening. Meanwhile, CafD exists predominantly in an inactive form because a conformational change of an aspartic acid induced by formation of an Asp-Arg pair acts as an on/off switch, which is inhibited by substitution of a glycine for an arginine.

In the present study, the crystal structures of CafA in the absence and presence of the potent inhibitor acetazolamide

were determined at 1.8 Å and 2.0 Å resolution, respectively. Together with our biochemical results, our findings establish the molecular basis for understanding the catalytic mechanism of the major β-CAs in *A. fumigatus*, as well as a possible strategy for developing new antifungal agents for the treatment of invasive aspergillosis.

MATERIALS AND METHODS

Cloning, expression, and purification of CafA
A codon-optimized gene encoding CafA (residues 75-287) of *A. fumigatus* was cloned between the *Eco*RI and *Not*I sites of the pGEX4T3 vector. This vector harbors a thrombin-cleavable N-terminal glutathione S-transferase. The resulting construct was transformed into *Escherichia coli* BL21 (DE3) cells, grown in Lysogeny Broth medium at 37°C. When the optical density at 600 nm (OD_{600}) reached 0.6-0.7, protein expression was induced with 1 mM isopropyl-β-d-thiogalactopyranoside (IPTG) for 16 h at 20°C.

After harvesting cells and lysing using a microfluidizer, CafA protein was purified using glutathione agarose beads (GoldBio, USA). After thorough washing, the protein was eluted by on-column thrombin cleavage in buffer containing 20 mM TRIS-HCl pH 8.0 and 200 mM NaCl. The protein was further purified by HiTrap Q anion exchange chromatography (GE Healthcare, USA) and Superdex 200 gel filtration chromatography (GE Healthcare). All purification steps were performed on ice or at 4°C.

CO_2 hydration activity
In vitro CO_2 hydration activity was measured using a modified electrometric method (Carter et al., 1969). Briefly, CO_2-saturated water was freshly prepared by bubbling CO_2 gas through water for at least 30 min. The reaction was initiated by addition of 4 ml CO_2-saturated water to 6 ml reaction buffer (20 mM TRIS-HCl pH 8.5) in the presence or absence of purified protein. Activity was monitored by recording the pH change from 8.3 to 6.3 at 5 s intervals, and was calculated in Wilbur–Anderson units (WAU) using the following formula: $WAU = (T0 − T) / T$, where T0 and T refer to the time in seconds taken in the absence and presence of the enzyme, respectively (Wilbur and Anderson, 1948). For acetazolamide or anion inhibition, protein samples were mixed with varying concentrations of acetazolamide or anions (Sigma-Aldrich, USA) for 1 h on ice before the CO_2 hydration assay. Each assay was performed in triplicate using the same enzyme preparation.

Measuring thermal and pH stability
To measure thermal stability, proteins were pretreated at temperatures from 22°C to 100°C for 15 min. To measure pH stability, 20 μl protein was incubated at 4°C for 4 h in 80 μl of 50 mM buffer at different pH values between 4 and 10. Remaining enzymatic activity was measured by *in vitro* CO_2 hydration assay as described above, and was expressed as a percentage of the maximal activity at 22°C and pH 7.

Crystallization, X-ray diffraction data collection, and structure determination

Purified CafA was concentrated to 15-20 mg/ml for crystallization. Crystals were obtained at 22°C by the sitting-drop vapor diffusion method in 0.1 M MES (or TRIS-HCl) pH 6.0-7.5, 24%-30% (w/v) polyethylene glycol 2000 monomethyl ether (PEG2000MME), and 0.2-0.4 M sodium acetate. For co-crystallization, acetazolamide (Sigma-Aldrich) was added to a concentrated solution of protein at a 10:1 molar ratio and incubated on ice for 30 min. Crystals of CafA were cryo-protected in reservoir solution supplemented with ethylene glycerol and then flash-frozen in liquid nitrogen. X-ray diffraction data were collected at beamline 7A of the Pohang Accelerator Laboratory (PAL, Korea). Datasets were indexed, integrated, and scaled using the HKL2000 program (Otwinowski and Minor, 1997). The CafA structure was determined by molecular replacement using the structure of β-CA CAS2 from the fungus *Sordaria macrospora* (Protein Data Bank [PDB] code 4O1K) as the search model (Lehneck et al., 2014; McCoy et al., 2007). Models were built by several cycles of manual modeling in COOT (Emsley and Cowtan, 2004), and were refined by REFMAC5 and PHENIX (Adams et al., 2010; Murshudov et al., 1997). X-ray crystallographic data and refinement statistics are summarized in Table 1. All residues lie in the allowed region of the Ramachandran plot. All figures in the manuscript were prepared using the program PyMOL (www.pymol.org).

Accession codes

Coordinates and structure factors for CafA have been deposited in the PDB under accession codes 7COI (apo, crystal form 1) and 7COJ (acetazolamide-bound, crystal form 2).

Table 1. X-ray data collection and refinement statistics

	CafA	
	Form1 (apo, PDB ID 7COI)	Form 2 (acetazolamide-bound, PDB ID 7COJ)
Data collection		
Space group	$P22_12_1$	$P22_12_1$
Cell dimensions		
a, b, c (Å)	66.6, 88.7, 144.2	66.9, 87.9, 144.7
α, β, γ (°)	90.0, 90.0, 90.0	90.0, 90.0, 90.0
Resolution (Å)	50.0-1.8 (1.83-1.80)	50.0-2.0 (2.07-2.00)
R_{pim}	0.03 (0.28)	0.03 (0.12)
I/σI	33.1 (4.7)	43.2 (10.5)
CC1/2	0.9 (0.9)	0.9 (0.9)
Completeness (%)	99.9 (100.0)	99.9 (100.0)
Redundancy	7.2 (7.2)	7.1 (7.2)
Refinement		
Resolution (Å)	50.0-1.8	50.0-2.0
No. of reflections (work/test)	76,053/4,066	55,669/2,919
R_{work}/R_{free}	17.2/20.4	16.3/20.4
No. of atoms		
Protein	6,400	6,436
Zinc	4	4
Acetazolamide	-	52
Acetate	16	-
Water	700	522
B factors		
Protein	25.7	31.3
Zinc	18.5	22.0
Acetazolamide	-	28.0
Acetate	28.6	-
Water	32.4	34.3
R.m.s. deviations		
Bond lengths (Å)	0.011	0.010
Bond angles (°)	1.625	1.682
Ramachandran plot (%)		
Most favored	90.5	91.4
Allowed	9.5	8.6
Generously allowed	0	0
Disallowed	0	0

Numbers in parentheses were calculated with data in the highest resolution shell.
R.m.s. deviations, root-mean-square deviations.

RESULTS AND DISCUSSION

CafA is a tetramer in solution

To investigate the oligomeric state of CafA in solution, the protein was expressed in bacteria and analyzed by size exclusion chromatography. Originally, we expressed full-length CafA, but it was expressed as two bands with similar densities as judged by sodium dodecyl sulfate polyacrylamide gel electrophoresis (SDS-PAGE) (Fig. 1A). CafA was predicted to be a mitochondrial protein processed to its mature form by cleavage of its N-terminal mitochondrial targeting sequence (Han et al., 2010); hence we thought that overexpression might reduce the efficiency of this process. Therefore, using the MitoFates program (Fukasawa et al., 2015), we constructed two truncated variants of CafA in which the mitochondrial targeting peptide was eliminated to achieve a homogenous product. Based on expression level, a construct comprising CafA residues 75-287 was chosen for further biochemical and crystallographic studies (Fig. 1A). The final CafA construct used in our experiments comprised 213 amino acids with a predicted molecular mass of 23 kDa. Analysis by size exclusion chromatography showed that CafA eluted as a single peak at a position corresponding to the expected molecular mass for a tetramer (92 kDa; Fig. 1B). The fact that the tetramers persisted during gel filtration chromatography suggests that their tetrameric configurations are stabilized by strong interfacial interactions.

CO$_2$ hydration activity, thermal and pH stability, and enzyme inhibition

To determine the catalytic activities of the purified enzyme, *in vitro* CO$_2$ hydration activities were measured by electrometric methods (Carter et al., 1969). CAs catalyze the efficient hydration of CO$_2$, and the hydrogen ions produced are released into the surrounding solvent, lowering its pH. Previously, we showed that CafA (20 WAU/mg) was active under our experimental conditions, with activity approximately 8-fold higher than that of CafC and CafD (2.4 WAU/mg), which are minor β-CAs in *A. fumigatus* (Kim et al., 2019a). However, CafA had much lower activity than the highly thermostable α-CAs from *Persephonella marina* EX-H1 (4,960 WAU/mg) (Kanth et al., 2014), *Thermovibrio ammonificans* (5,236 WAU/mg) (James et al., 2014), and *Sulfurihydrogenibium yellowstonense* YO3AOP1 (7,254 WAU/mg) (Capasso et al., 2012a).

Next, we explored the thermal and pH stability of CafA. As shown in Fig. 2A, CafA retained > 70% of its initial activity after incubation at temperatures up to 40°C, although it retained only 30% activity after 50°C treatment, and activity was almost negligible after exposure to temperatures above 50°C. To test the effect of pH on enzyme activity, proteins were pre-incubated in solutions with different pH values (pH 4-10). CafA was stable over a wide pH range (pH 5-9), but was rapidly inactivated below pH 5 or above pH 10 (Fig. 2B). This is reminiscent of previous studies showing that *A. fumigatus* can survive in neutral or alkaline environments, but not under acidic growth conditions (Amich et al., 2010).

Acetazolamide is a potent sulfonamide-based CA inhibitor. Its inhibition of enzymatic activity of CAs has been studied extensively as CAs are essential for the survival of many cancer cells under acidic and hypoxic stress (Neri and Supuran, 2011). Recently anions were also shown to inhibit the catalytic activity of fungal β-CAs (Innocenti et al., 2008; 2009; Isik et al., 2008). To determine the effect of anions on the activities of CafA, various concentrations of nitrate (NO$_3^-$), nitrite (NO$_2^-$), and sulfate (SO$_4^{2-}$) ions were separately added, and mixtures were incubated on ice for 30 min before measuring
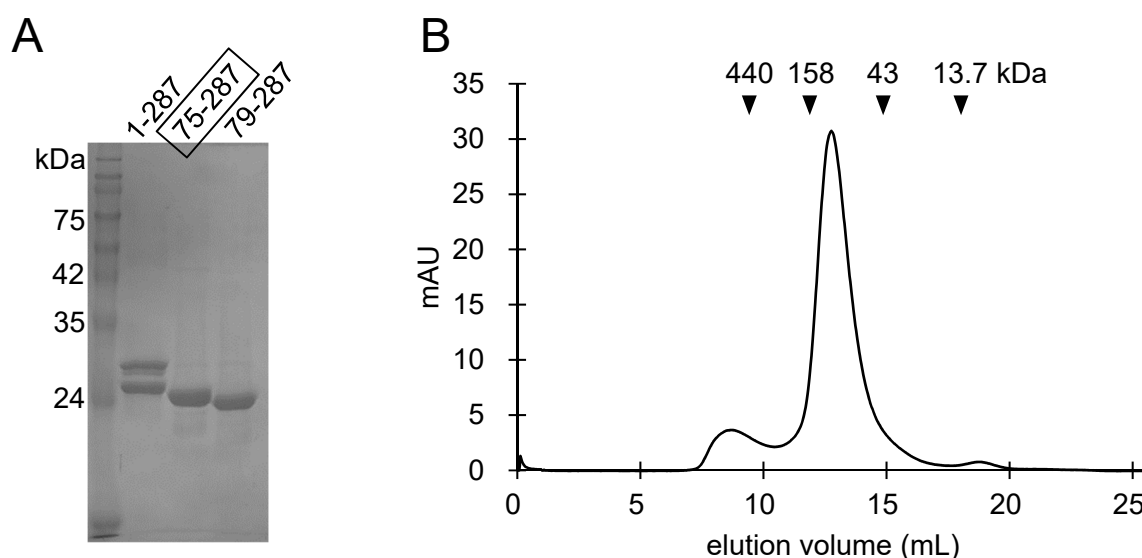

Fig. 1. Analysis of purified proteins by SDS-PAGE and gel filtration chromatography. (A) SDS-PAGE analysis of full-length (1-287) and truncated (75-287 and 79-287) variants of CafA. Constructs used in this study are enclosed in a black box. (B) Elution profile of CafA obtained using a Superdex Increase 200 10/300 GL column. The molecular weight of CafA was estimated by comparison with gel filtration standards (black arrows) ferritin (440 kDa), aldolase (158 kDa), ovalbumin (43 kDa), and ribonuclease A (13.7 kDa).
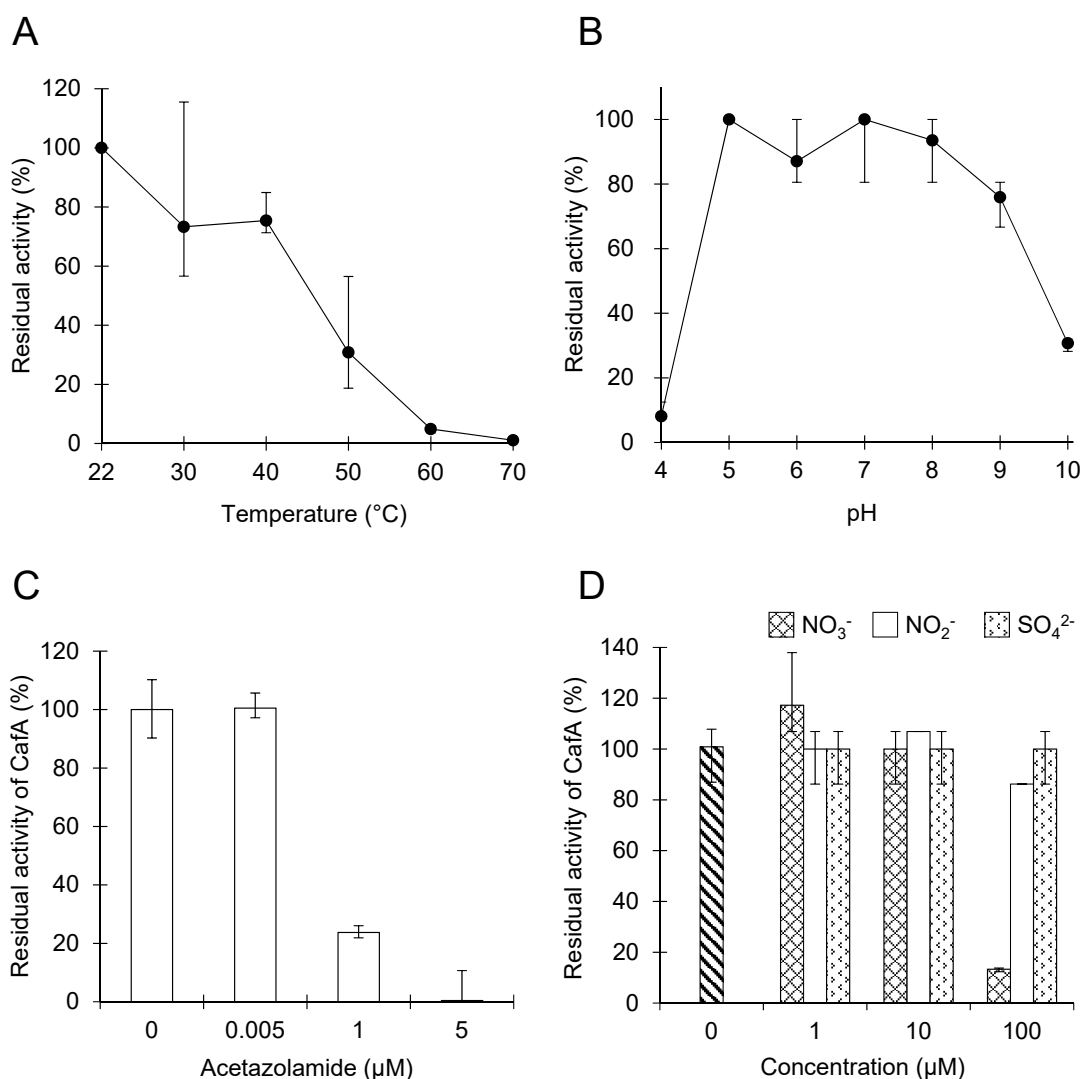
A

B

C

D

Fig. 2. Biochemical characterization. (A) Thermal and (B) pH stability of purified CafA. CO_2 hydration activities of purified CafA were obtained by measuring pH over time. Each point is the mean of three separate replicate experiments, and error bars represent SD. Maximum activities at 22°C and pH 7.0 were set as 100% in (A) and (B), respectively. (C) Inhibition of CafA with various concentrations of acetazolamide. CO_2 hydration activity without acetazolamide was set at 100%. (D) Inhibition of CafA by anions.

CO_2 hydration. Acetazolamide was used as a positive control. As expected, CafA activity was reduced by increasing the acetazolamide concentration and was completely inhibited at 5 µM acetazolamide (Fig. 2C). Interestingly, CafA was also weakly inhibited by nitrate in the submillimolar range (Fig. 2D). By contrast, nitrogen dioxide and sulfate had no inhibitory effect over the concentration ranges tested. This result suggests that nitrate or nitrate-containing compounds may represent a promising class of antifungal agents for the treatment of invasive aspergillosis (Supuran, 2008).

Overall enzyme structure

To establish the structural basis for the catalytic activity of CafA, we crystallized the purified protein in the presence and absence of acetazolamide, and determined the structures by X-ray crystallography (Table 1). Residues of the N-terminus

(75-76), the linker region (97-101 and 269-275), and the C-terminus (286-287) could not be fitted effectively into the electron density map and were therefore not included in the final model. In our structure, CafA forms a plant-type tetramer from a dimer of dimers in the asymmetric unit, consistent with the gel filtration data (Figs. 1B and 3A). We observed that tetramerization is driven by the association of pairs of relatively flat surfaces composed of α-helices orthogonal to the dimerization interfaces. CafA possess the typical structural features of other plant-type β-CAs (Figs. 3B and 4) (Cronk et al., 2006; Dostál et al., 2018; Lehneck et al., 2014; Schlicker et al., 2009). The overall structure of each protomer consists of three parts: an N-terminal α-helical extension, a conserved central core comprising 10 α-helices and 5 β-strands, and a C-terminal subdomain (Fig. 3B). The N-terminal α-helix, which includes two perpendicularly oriented helices, extends
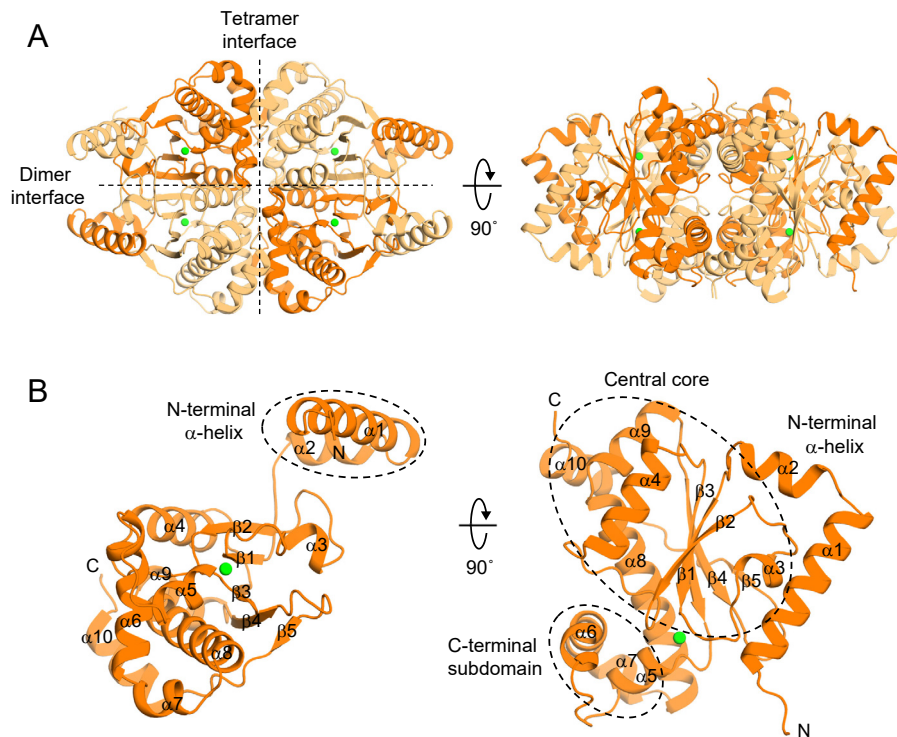
Fig. 3. The molecular architecture of CafA. (A) Cartoon representation of the CafA tetramer. Zinc ions are shown as green spheres. (B) CafA protomer structure. Subdomains within the protomer are indicated by black dashed circles.
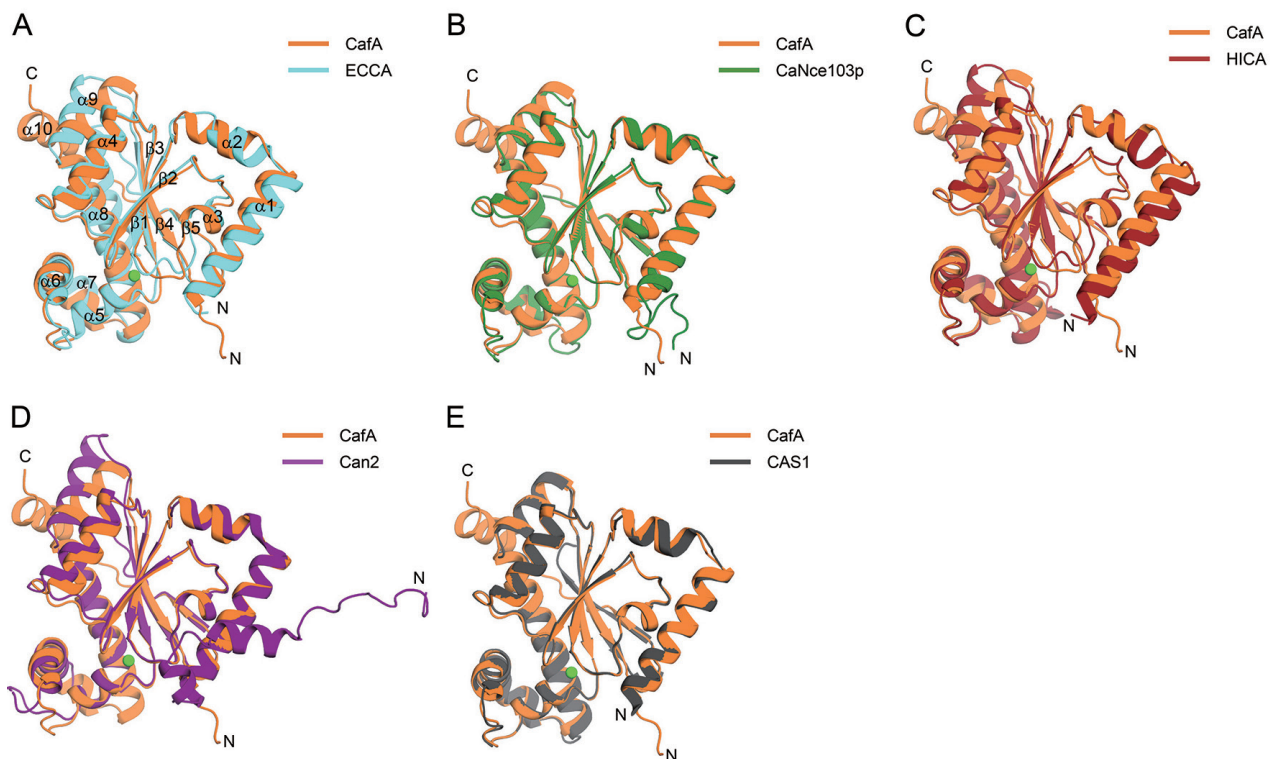

Fig. 4. Structural comparison of CafA and other plant-type β-CAs. Superimposition of one protomer of CafA onto one protomer of other β-CAs from (A) *Escherichia coli* (ECCA, PDB ID 2ESF), (B) *Candida albicans* (CaNce103p, PDB ID 6GWU), (C) *Haemophilus influenza* (HICA, PDB ID 2A8D), (D) *Cryptococcus neoformans* (Can2, PDB ID 2W3Q), and (E) *Sordaria macrospora* (CAS1, PDB ID 4O1J).

far out from the central core region, spanning the neighboring protomer and stabilizing dimer interface interactions. The core structures are composed of four parallel β-strands (β2-β1-β3-β4) accompanied by a fifth antiparallel β-strand (β5). The C-terminal subdomains flank the adjacent protomers, creating new contacts, thus further stabilizing tetramer formation. Structure-based sequence alignment showed that CafA shares a high degree of amino acid conservation with CafB, suggesting that they might share a similar protein fold and catalytic mechanism (Fig. 5). Note that throughout this article, single apostrophes are used to differentiate residues from the other protomer of the dimer.

The CafA active site

CafA (form 1) has a typical Type-I or open conformation in which the substrate binds at the dimer interface (Fig. 6). The catalytic zinc ion is tetrahedrally coordinated by three conserved residues (C119, H175, C178) and an acetate anion presumably acquired from the crystallization solution that replaces zinc-bound water in the metal coordination sphere (Fig. 6). The carboxyl group of acetate is firmly positioned by strong hydrogen bonds with the side chains of D121 and Q110' and the backbone nitrogen of G179. By contrast, the methyl group of acetate is oriented toward the hydrophobic side of the dimer interface composed of I143, F138', and F160'. The highly conserved D121 also forms essential salt bridges with R123 (the Asp-Arg pair).

We also solved the crystal structure of CafA in complex with acetazolamide (form 2) (Fig. 7A). The binding mode of acetazolamide is similar to that reported previously for β-CAs (Huang et al., 2011). The sulfonamide group of acetazolamide is directly bound to the zinc ion, replacing the native water molecule in the zinc coordination sphere, indicating that this conformation is catalytically inactive (Figs. 7B and

7C). The amide and hydroxyl groups of the sulfonamide motif form hydrogen bonds with the side chains of D121 and Q110', respectively, while the nitrogen atom of the acetyl-amide group interacts with the backbone oxygen of G179. The thiadiazole ring is sandwiched between G179 and F160'. Comparison of the CafA structures with and without acetazolamide reveals minor differences in this sandwich region; in the presence of the inhibitor, the phenyl ring of F160' undergoes a ~40° rotation, and G179 moves ~0.6 Å away from the thiadiazole ring to avoid steric clashes with the
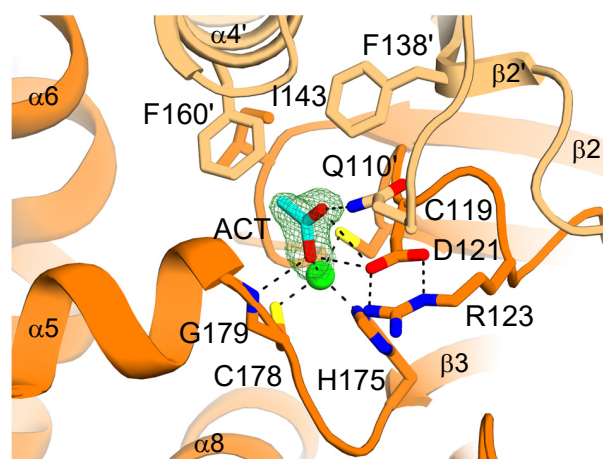

Fig. 6. The CafA active site. Close-up view of the zinc coordination sphere. Residues and the zinc-bound acetate (ACT) are shown in stick representation, while zinc ions are shown as green spheres. The Fo-Fc map superimposed on the refined acetate is contoured at the 3 σ level.

Fig. 5. Sequence alignment and secondary structure. N-terminal residues (1-74) that were not included in the CafA construct are colored gray. Secondary structural features are shown above the sequence alignment; α-helices are indicated as cylinders and β-strands as arrows. Residues responsible for zinc ion coordination in CafA and CafB are highlighted in yellow.
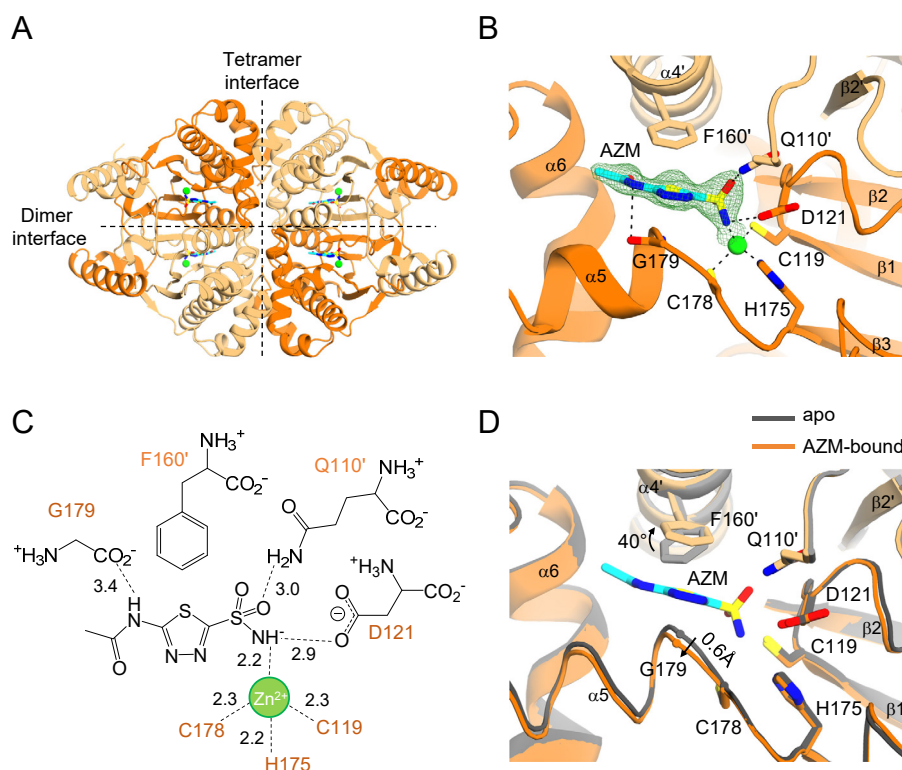
Fig. 7. The acetazolamide-bound CafA. (A) Cartoon representation of the acetazolamide-bound CafA tetramer. Zinc ions are shown as green spheres. The carbons, nitrogens, oxygens, and sulfurs of the acetazolamide (AZM) are colored cyan, blue, red, and yellow, respectively. (B) Active site of acetazolamide-bound CafA. The Fo-Fc map superimposed on the refined AZM map is contoured at the 2.3 σ level. (C) Schematic diagram of the CafA-AZM interactions. Residues engaging in hydrogen bonds and salt bridges with AZM are shown. The pH of the buffer and previous biochemical data suggest that the nitrogen atom of the sulfonamide moiety and the carboxyl group of D121 are likely to be deprotonated (Dollery, 1991). All distances are shown in angstroms. (D) Superimposition of the CafA active sites in the presence and absence of AZM. Structural changes in G179 and F160' are marked by black arrows. The α5 helix is drawn as a coil for clarity.

bound acetazolamide (Fig. 7D). It is noteworthy that no local conformational changes are induced in α-CAs by binding of acetazolamide due to their large active sites, which are fully exposed to the solvent (Eriksson et al., 1988; James et al., 2014; Nair et al., 1995).

In summary, the structure of CafA reveals key features that may be responsible for its apparent *in vitro* CO_2 hydration activity. The effect of pH on the activity of CafA suggests that *A. fumigatus* may use different catalytic strategies to regulate enzyme reactions in a pH-dependent manner. Importantly, knowledge of the structure of CafA in complex with acetazolamide and its functional intolerance of nitrate ions could be exploited to develop a promising class of antifungal agents for the treatment of invasive aspergillosis.

ACKNOWLEDGMENTS

AUTHOR CONTRIBUTIONS

All authors contributed to the study design, performed experiments, and interpreted the data. S.K., J.Y., and J.S. purified and crystallized the protein. S.K. and J.Y. performed enzyme activity assays. S.K. determined the crystal structures. S.K. and J.Y. prepared the figures. S.K. and M.S.J. wrote the manuscript. All authors helped to improve the manuscript and approved the final version.

CONFLICT OF INTEREST

The authors have no potential conflicts of interest to disclose.

ORCID

Subin Kim   https://orcid.org/0000-0003-2441-6847
Jungyoon Yeon   https://orcid.org/0000-0001-6238-487X
Jongmin Sung   https://orcid.org/0000-0003-3490-3948
Mi Sun Jin   https://orcid.org/0000-0003-0516-0284

REFERENCES

Adams, P.D., Afonine, P.V., Bunkóczi, G., Chen, V.B., Davis, I.W., Echols, N., Headd, J.J., Hung, L.W., Kapral, G.J., Grosse-Kunstleve, R.W., et al. (2010). PHENIX: a comprehensive Python-based system for macromolecular

structure solution. Acta Crystallogr. D Biol. Crystallogr. *66*, 213-221.

Alterio, V., Hilvo, M., Di Fiore, A., Supuran, C.T., Pan, P., Parkkila, S., Scaloni, A., Pastorek, J., Pastorekova, S., Pedone, C., et al. (2009). Crystal structure of the catalytic domain of the tumor-associated human carbonic anhydrase IX. Proc. Natl. Acad. Sci. U. S. A. *106*, 16233-16238.

Amich, J., Vicentefranqueira, R., Leal, F., and Calera, J.A. (2010). Aspergillus fumigatus survival in alkaline and extreme zinc-limiting environments relies on the induction of a zinc homeostasis system encoded by the zrfC and aspf2 genes. Eukaryot. Cell *9*, 424-437.

Bahn, Y.S., Cox, G.M., Perfect, J.R., and Heitman, J. (2005). Carbonic anhydrase and CO2 sensing during Cryptococcus neoformans growth, differentiation, and virulence. Curr. Biol. *15*, 2013-2020.

Capasso, C., De Luca, V., Carginale, V., Cannio, R., and Rossi, M. (2012a). Biochemical properties of a novel and highly thermostable bacterial alpha-carbonic anhydrase from Sulfurihydrogenibium yellowstonense YO3AOP1. J. Enzyme Inhib. Med. Chem. *27*, 892-897.

Capasso, C., De Luca, V., Carginale, V., Caramuscio, P., Cavalheiro, C., Cannio, R., and Rossi, M. (2012b). Characterization and properties of a new thermoactive and thermostable carbonic anhydrase. Chem. Eng. Trans. *27*, 271-276.

Carter, J.M., Havard, D.J., and Parsons, D.S. (1969). Electrometric assay of rate of hydration of CO2 for investigation of kinetics of carbonic anhydrase. J. Physiol. *204*, 60P-62P.

Cronk, J.D., Rowlett, R.S., Zhang, K.Y., Tu, C., Endrizzi, J.A., Lee, J., Gareiss, P.C., and Preiss, J.R. (2006). Identification of a novel noncatalytic bicarbonate binding site in eubacterial beta-carbonic anhydrase. Biochemistry *45*, 4351-4361.

Del Prete, S., Vullo, D., Fisher, G.M., Andrews, K.T., Poulsen, S.A., Capasso, C., and Supuran, C.T. (2014a). Discovery of a new family of carbonic anhydrases in the malaria pathogen Plasmodium falciparum--the eta-carbonic anhydrases. Bioorg. Med. Chem. Lett. *24*, 4389-4396.

Del Prete, S., Vullo, D., Scozzafava, A., Capasso, C., and Supuran, C.T. (2014b). Cloning, characterization and anion inhibition study of the delta-class carbonic anhydrase (TweCA) from the marine diatom Thalassiosira weissflogii. Bioorg. Med. Chem. *22*, 531-537.

Dollery, C.T. (1991). Therapeutic Drugs (Edinburgh; London: Churchill Livingstone).

Dostál, J., Brynda, J., Blaha, J., Machacek, S., Heidingsfeld, O., and Pichová, I. (2018). Crystal structure of carbonic anhydrase CaNce103p from the pathogenic yeast Candida albicans. BMC Struct. Biol. *18*, 14.

Elleuche, S. and Pöggeler, S. (2009). Evolution of carbonic anhydrases in fungi. Curr. Genet. *55*, 211-222.

Elleuche, S. and Pöggeler, S. (2010). Carbonic anhydrases in fungi. Microbiology *156*, 23-29.

Emsley, P. and Cowtan, K. (2004). Coot: model-building tools for molecular graphics. Acta Crystallogr. D Biol. Crystallogr. *60*, 2126-2132.

Eriksson, A.E., Jones, T.A., and Liljas, A. (1988). Refined structure of human carbonic anhydrase II at 2.0 A resolution. Proteins *4*, 274-282.

Fisher, S.Z., Maupin, C.M., Budayova-Spano, M., Govindasamy, L., Tu, C., Agbandje-McKenna, M., Silverman, D.N., Voth, G.A., and McKenna, R. (2007). Atomic crystal and molecular dynamics simulation structures of human carbonic anhydrase II: insights into the proton transfer mechanism. Biochemistry *46*, 2930-2937.

Fukasawa, Y., Tsuji, J., Fu, S.C., Tomii, K., Horton, P., and Imai, K. (2015). MitoFates: improved prediction of mitochondrial targeting sequences and their cleavage sites. Mol. Cell. Proteomics *14*, 1113-1126.

Götz, R., Gnann, A., and Zimmermann, F.K. (1999). Deletion of the carbonic anhydrase-like gene NCE103 of the yeast Saccharomyces cerevisiae causes an oxygen-sensitive growth defect. Yeast *15*, 855-864.

Han, K.H., Chun, Y.H., Figueiredo Bde, C., Soriani, F.M., Savoldi, M., Almeida, A., Rodrigues, F., Cairns, C.T., Bignell, E., Tobal, J.M., et al. (2010). The conserved and divergent roles of carbonic anhydrases in the filamentous fungi Aspergillus fumigatus and Aspergillus nidulans. Mol. Microbiol. *75*, 1372-1388.

Huang, S., Hainzl, T., Grundström, C., Forsman, C., Samuelsson, G., and Sauer-Eriksson, A.E. (2011). Structural studies of beta-carbonic anhydrase from the green alga Coccomyxa: inhibitor complexes with anions and acetazolamide. PLoS One *6*, e28458.

Innocenti, A., Leewattanapasuk, W., Mühlschlegel, F.A., Mastrolorenzo, A., and Supuran, C.T. (2009). Carbonic anhydrase inhibitors. Inhibition of the beta-class enzyme from the pathogenic yeast Candida glabrata with anions. Bioorg. Med. Chem. Lett. *19*, 4802-4805.

Innocenti, A., Mühlschlegel, F.A., Hall, R.A., Steegborn, C., Scozzafava, A., and Supuran, C.T. (2008). Carbonic anhydrase inhibitors: inhibition of the beta-class enzymes from the fungal pathogens Candida albicans and Cryptococcus neoformans with simple anions. Bioorg. Med. Chem. Lett. *18*, 5066-5070.

Isik, S., Kockar, F., Arslan, O., Guler, O.O., Innocenti, A., and Supuran, C.T. (2008). Carbonic anhydrase inhibitors. Inhibition of the beta-class enzyme from the yeast Saccharomyces cerevisiae with anions. Bioorg. Med. Chem. Lett. *18*, 6327-6331.

Iverson, T.M., Alber, B.E., Kisker, C., Ferry, J.G., and Rees, D.C. (2000). A closer look at the active site of gamma-class carbonic anhydrases: high-resolution crystallographic studies of the carbonic anhydrase from Methanosarcina thermophila. Biochemistry *39*, 9222-9231.

James, P., Isupov, M.N., Sayer, C., Saneei, V., Berg, S., Lioliou, M., Kotlar, H.K., and Littlechild, J.A. (2014). The structure of a tetrameric alpha-carbonic anhydrase from Thermovibrio ammonificans reveals a core formed around intermolecular disulfides that contribute to its thermostability. Acta Crystallogr. D Biol. Crystallogr. *70*, 2607-2618.

Jo, B.H., Seo, J.H., and Cha, H.J. (2014). Bacterial extremo-α-carbonic anhydrases from deep-sea hydrothermal vents as potential biocatalysts for CO2 sequestration. J. Mol. Catal. B Enzym. *109*, 31-39.

Kanth, B.K., Jun, S.Y., Kumari, S., and Pack, S.P. (2014). Highly thermostable carbonic anhydrase from Persephonella marina EX-H1: its expression and characterization for CO2-sequestration applications. Process Biochem. *49*, 2114-2121.

Kikutani, S., Nakajima, K., Nagasato, C., Tsuji, Y., Miyatake, A., and Matsuda, Y. (2016). Thylakoid luminal theta-carbonic anhydrase critical for growth and photosynthesis in the marine diatom Phaeodactylum tricornutum. Proc. Natl. Acad. Sci. U. S. A. *113*, 9828-9833.

Kim, S., Kim, N.J., Hong, S., Kim, S., Sung, J., and Jin, M.S. (2019a). The structural basis of the low catalytic activities of the two minor beta-carbonic anhydrases of the filamentous fungus Aspergillus fumigatus. J. Struct. Biol. *208*, 61-68.

Kim, S., Sung, J., Yeon, J., Choi, S.H., and Jin, M.S. (2019b). Crystal structure of a highly thermostable alpha-carbonic anhydrase from Persephonella marina EX-H1. Mol. Cells *42*, 460-469.

Kimber, M.S. and Pai, E.F. (2000). The active site architecture of Pisum sativum beta-carbonic anhydrase is a mirror image of that of alpha-carbonic anhydrases. EMBO J. *19*, 1407-1418.

Klengel, T., Liang, W.J., Chaloupka, J., Ruoff, C., Schröppel, K., Naglik, J.R., Eckert, S.E., Mogensen, E.G., Haynes, K., Tuite, M.F., et al. (2005). Fungal adenylyl cyclase integrates CO2 sensing with cAMP signaling and virulence. Curr. Biol. *15*, 2021-2026.

Lehneck, R., Neumann, P., Vullo, D., Elleuche, S., Supuran, C.T., Ficner, R., and Pöggeler, S. (2014). Crystal structures of two tetrameric beta-carbonic anhydrases from the filamentous ascomycete Sordaria macrospora. FEBS J. *281*, 1759-1772.

Luca, V.D., Vullo, D., Scozzafava, A., Carginale, V., Rossi, M., Supuran, C.T., and Capasso, C. (2013). An α-carbonic anhydrase from the thermophilic bacterium Sulphurihydrogenibium azorense is the fastest enzyme known for the CO2 hydration reaction. Bioorg Med. Chem. *21*, 1465-1469.

Maupin, C.M. and Voth, G.A. (2007). Preferred orientations of His64 in human carbonic anhydrase II. Biochemistry *46*, 2938-2947.

McCoy, A.J., Grosse-Kunstleve, R.W., Adams, P.D., Winn, M.D., Storoni, L.C., and Read, R.J. (2007). Phaser crystallographic software. J. Appl. Crystallogr. *40*, 658-674.

Meldrum, N.U. and Roughton, F.J. (1933). Carbonic anhydrase. Its preparation and properties. J. Physiol. *80*, 113-142.

Mitsuhashi, S., Mizushima, T., Yamashita, E., Yamamoto, M., Kumasaka, T., Moriyama, H., Ueki, T., Miyachi, S., and Tsukihara, T. (2000). X-ray structure of beta-carbonic anhydrase from the red alga, Porphyridium purpureum, reveals a novel catalytic site for CO(2) hydration. J. Biol. Chem. *275*, 5521-5526.

Murshudov, G.N., Vagin, A.A., and Dodson, E.J. (1997). Refinement of macromolecular structures by the maximum-likelihood method. Acta Crystallogr. D Biol. Crystallogr. *53*, 240-255.

Nair, S.K., Krebs, J.F., Christianson, D.W., and Fierke, C.A. (1995). Structural basis of inhibitor affinity to variants of human carbonic anhydrase II. Biochemistry *34*, 3981-3989.

Neish, A.C. (1939). Studies on chloroplasts: their chemical composition and the distribution of certain metabolites between the chloroplasts and the remainder of the leaf. Biochem. J. *33*, 300-308.

Neri, D. and Supuran, C.T. (2011). Interfering with pH regulation in tumours as a therapeutic strategy. Nat. Rev. Drug Discov. *10*, 767-777.

Otwinowski, Z. and Minor, W. (1997). Processing of X-ray diffraction data collected in oscillation mode. Methods Enzymol. *276*, 307-326.

Pilka, E.S., Kochan, G., Oppermann, U., and Yue, W.W. (2012). Crystal structure of the secretory isozyme of mammalian carbonic anhydrases CA VI: implications for biological assembly and inhibitor development. Biochem. Biophys. Res. Commun. *419*, 485-489.

Ren, P., Chaturvedi, V., and Chaturvedi, S. (2014). Carbon dioxide is a powerful inducer of monokaryotic hyphae and spore development in Cryptococcus gattii and carbonic anhydrase activity is dispensable in this dimorphic transition. PLoS One *9*, e113147.

Russo, M.E., Scialla, S., De Luca, V., Capasso, C., Olivieri, G., and Marzocchella, A. (2013). Immobilization of carbonic anhydrase for biomimetic CO2 capture. Chem. Eng. Trans. *32*, 1867-1872.

Schlicker, C., Hall, R.A., Vullo, D., Middelhaufe, S., Gertz, M., Supuran, C.T., Mühlschlegel, F.A., and Steegborn, C. (2009). Structure and inhibition of the CO2-sensing carbonic anhydrase Can2 from the pathogenic fungus Cryptococcus neoformans. J. Mol. Biol. *385*, 1207-1220.

Silverman, D.N. and Lindskog, S. (1988). The catalytic mechanism of carbonic anhydrase: implications of a rate-limiting protolysis of water. Acc. Chem. Res. *21*, 30-36.

Smith, K.S. and Ferry, J.G. (1999). A plant-type (beta-class) carbonic anhydrase in the thermophilic methanoarchaeon Methanobacterium thermoautotrophicum. J. Bacteriol. *181*, 6247-6253.

Smith, K.S., Jakubzick, C., Whittam, T.S., and Ferry, J.G. (1999). Carbonic anhydrase is an ancient enzyme widespread in prokaryotes. Proc. Natl. Acad. Sci. U. S. A. *96*, 15184-15189.

Strop, P., Smith, K.S., Iverson, T.M., Ferry, J.G., and Rees, D.C. (2001). Crystal structure of the "cab"-type beta class carbonic anhydrase from the archaeon Methanobacterium thermoautotrophicum. J. Biol. Chem. *276*, 10299-10305.

Supuran, C.T. (2008). Carbonic anhydrases: novel therapeutic applications for inhibitors and activators. Nat. Rev. Drug Discov. *7*, 168-181.

Supuran, C.T. (2016). Structure and function of carbonic anhydrases. Biochem. J. *473*, 2023-2032.

West, D., Kim, C.U., Tu, C., Robbins, A.H., Gruner, S.M., Silverman, D.N., and McKenna, R. (2012). Structural and kinetic effects on changes in the CO(2) binding pocket of human carbonic anhydrase II. Biochemistry *51*, 9156-9163.

Whittington, D.A., Waheed, A., Ulmasov, B., Shah, G.N., Grubb, J.H., Sly, W.S., and Christianson, D.W. (2001). Crystal structure of the dimeric extracellular domain of human carbonic anhydrase XII, a bitopic membrane protein overexpressed in certain cancer tumor cells. Proc. Natl. Acad. Sci. U. S. A. *98*, 9545-9550.

Wilbur, K.M. and Anderson, N.G. (1948). Electrometric and colorimetric determination of carbonic anhydrase. J. Biol. Chem. *176*, 147-154.

Xu, Y., Feng, L., Jeffrey, P.D., Shi, Y., and Morel, F.M. (2008). Structure and metal exchange in the cadmium carbonic anhydrase of marine diatoms. Nature *452*, 56-61.